Linear and nonlinear benchmarks between the CLT code and the M3D-C1 code for the 2/1 resistive tearing mode and the 1/1 resistive kink mode ☆

W. Zhang [a], S.C. Jardin [b], Z.W. Ma [a,*], A. Kleiner [b], H.W. Zhang [a]

[a] *Institute for Fusion Theory and Simulation, Department of Physics, Zhejiang University, Hangzhou 310027, China*
[b] *Princeton Plasma Physics Laboratory, P.O. Box 451, Princeton, NJ 08543, USA*

ARTICLE INFO

ABSTRACT

The linear and nonlinear benchmarks between the CLT code and the M3D-C1 code for the 2/1 resistive tearing mode and the 1/1 resistive kink mode are presented. CLT is an explicit finite difference code, while M3D-C1 is an implicit finite element code. Although the implementations of CLT and M3D-C1 are totally different, we find that the simulation results of the resistive-kink mode and the $m/n = 2/1$ tearing mode from M3D-C1 and CLT are almost the same, including the linear and nonlinear growth rates, the mode structures, the nonlinear saturation levels, the Poincare plots, and the scaling laws. This confirms that the nonlinear results for the 1/1 resistive-kink mode and 2/1 tearing mode are accurate and reliable.

© 2021 Elsevier B.V. All rights reserved.

1. Introduction

Tearing modes are a common phenomenon in tokamaks. The tearing modes are the primary cause of the degradation of tokamak performance [1] and even disruptions [2]. Sawteeth, which not only flatten the plasma temperature but also may trigger neoclassical tearing modes in nearby resonant surfaces [3,4], are believed to be related to the nonlinear evolution of the resistive-kink mode [5,6]. It is worthwhile to investigate these instabilities to increase our understanding to achieve high-performance operation in future fusion reactors [7,8].

The resistive tearing mode was first studied by Furth et al., who found that the linear growth rate asymptotically scales like $\gamma \sim S^{-3/5}$, where S is the Lundquist number [9]. The first analytical theory of the resistive-kink mode was given by Coppi et al. [6], who found that the linear growth rate asymptotically scales like $\gamma \sim S^{-1/3}$. Not only linear but also nonlinear theoretical studies have been reported in the past decades [10–12]. It should be noted that significant simplifications of the physical model and the

geometry are applied in these analytical studies. Simulation studies have been widely performed [13,14] to confirm that these assumptions are reasonable and gain more insight into those instabilities. Since the implementations of different codes are different [15–19], and the nonlinear evolution from different simulation codes sometimes is significantly different, it is difficult to say which simulations are accurate and reliable.

One way to verify the simulation results is to benchmark between different codes. This method can be useful, but it is still a challenge since the nonlinear simulation results can be sensitive to many details of the formulation, the equilibrium, the boundary conditions, and the initial conditions. The M3D-C1 code is an implicit, three-dimensional, high-order finite-element code for the solution of the time-dependent linear or nonlinear two-fluid magnetohydrodynamic (MHD) equations in cylindrical or toroidal geometry [17]. The CLT code is an explicit three-dimensional finite-difference nonlinear MHD code for toroidal geometry [19]. Although they are both used to investigate MHD instabilities in tokamaks, the implementations of the two codes are totally different. Benchmarking the two codes on different MHD instabilities could demonstrate that the simulation results of both codes are accurate and reliable. Benchmarks between M3D-C1 and other MHD codes on the linear tearing instabilities [20], the vertical displacement [21], the impurity dynamics [22,23], the linear growth rate of the edge localized modes [24], and plasma's linear response to resonant magnetic perturbations (RMPs) [25] have been performed.

The classification of points in CLT
(only the z direction is plotted)
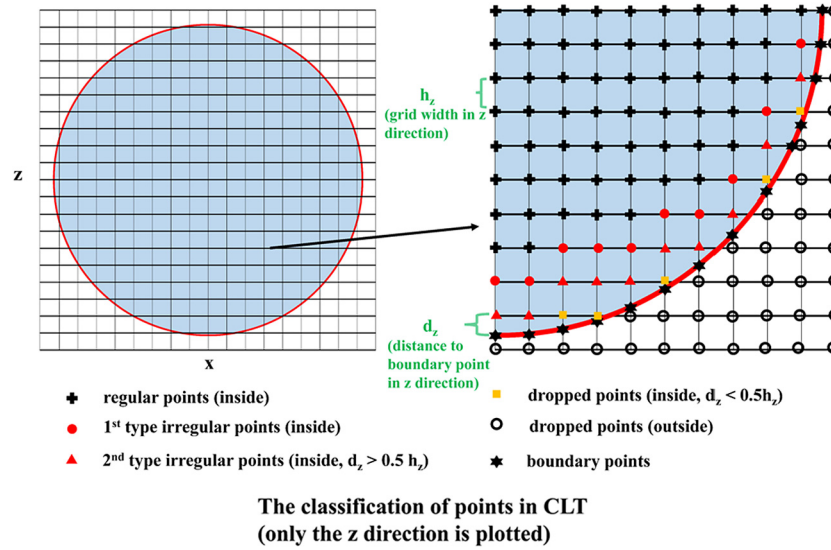
Fig. 1. The schematic diagram of the cut-cell method. The grids are divided into 6 types, i.e. regular point: 4th order central finite difference (5 points, the boundary points are not required); 1st type irregular points: 4th order bias finite difference (5 points, the values at the boundary points are required); 2nd type irregular points: 4th order central finite difference (5 points, the values at the boundary points and the 1st type irregular points are required); dropped points (inside, $d_z < 0.5h_Z$): not calculated in the specified dropped direction (because it is too close to the boundary point), but will be updated by linear interpolation for the requirement in another direction; dropped points (outside): not calculated; boundary points: fixed boundary condition is used at present, it will be updated to free boundary condition in the future.

Since CLT is newly developed, we have just finished the benchmark with MARS-F [26] on plasma's linear response to RMPs [27]. The nonlinear benchmarks between CLT and other MHD codes are needed. In the present paper, the benchmarks between CLT and M3D-C1, including the linear and nonlinear evolutions of the tearing modes and the resistive-kink mode, are presented.

2. Model descriptions, normalizations, and code implementations

A brief introduction of the two codes is presented in this subsection. It should be noted that both of the codes could include two-fluid MHD effects. In the present paper, we only use the single-fluid model; a benchmark with the two-fluid MHD model will be the subject of future work.

The single-fluid MHD model used in CLT [19] and M3D-C1 [28]. is as follows:

$$\frac{\partial \rho}{\partial t} = -\nabla \cdot (\rho \mathbf{v}) + \nabla \cdot [D\nabla(\rho - \rho_0)] \tag{1.1}$$

$$\frac{\partial p}{\partial t} = -\mathbf{v} \cdot \nabla p - \Gamma p \nabla \cdot \mathbf{v} + \nabla \cdot [\kappa_\perp \nabla_\perp (p - p_0)] + \nabla \cdot [\kappa_{||} \nabla_{||} p] \tag{1.2}$$

$$\frac{\partial \mathbf{v}}{\partial t} = -\mathbf{v} \cdot \nabla \mathbf{v} + (\mathbf{J} \times \mathbf{B} - \nabla p)/\rho + \nabla \cdot [\nu \nabla(\mathbf{v})] \tag{1.3}$$

$$\frac{\partial \mathbf{B}}{\partial t} = -\nabla \times \mathbf{E} \tag{1.4}$$

$$\mathbf{E} = -\mathbf{v} \times \mathbf{B} + \eta(\mathbf{J} - \mathbf{J}_0) \tag{1.5}$$

$$\mathbf{J} = \frac{1}{\mu_0} \nabla \times \mathbf{B}. \tag{1.6}$$

Here ρ, p, $\mathbf{v}$, $\mathbf{B}$, $\mathbf{E}$, and $\mathbf{J}$ are the mass density, the plasma pressure, the velocity, magnetic field, the electric field, and the current density, respectively. p_0, ρ_0, and $\mathbf{J_0}$ are the equilibrium plasma pressure, density, and current density, respectively. $\Gamma(= 5/3)$ is the ratio of specific heat of the plasma. Note that M3D-C1 actually time-advances the magnetic vector potential, $\mathbf{A}$, and not $\mathbf{B}$, but by taking the curl of the $\mathbf{A}$ equation, we obtain Eq. (1.4).

All variables are normalized as follows: $\mathbf{x}/L_0 \to \mathbf{x}$, $\rho/(n_0 M_i) \to \rho$, $p/(B_{00}^2/\mu_0) \to p$, $t/t_A \to t$, $\mathbf{v}/v_A \to \mathbf{v}$, $\mathbf{B}/B_{00} \to \mathbf{B}$, $\mathbf{E}/(v_A B_{00}) \to \mathbf{E}$, and $\mathbf{J}/(B_{00}/\mu_0 a) \to \mathbf{J}$ where $L_0 = 1$ m is the normal length,

$B_{00} = 1$ T is the normal strength of the magnetic field, $n_0 = 1 \times 10^{20}$ m^{-3} is the normal particle density, M_i is the mass of the ion, $v_A = B_{00}/\sqrt{\mu_0 n_0 M_i}$ is the Alfvén speed, and $t_A = L_0/v_A$ is the Alfvén time. The resistivity η and the diffusion coefficient D, the perpendicular and parallel thermal conductivity $\kappa_\perp$ and $\kappa_{||}$, the viscosity ν are normalized as follows: $\eta/(\mu_0 L_0^2/t_A) \to \eta$, $D/(L_0^2/t_A) \to D$, $\kappa_\perp/(L_0^2/t_A) \to \kappa_\perp$, $\kappa_{||}/(L_0^2/t_A) \to \kappa_{||}$, and $\nu/(L_0^2/t_A) \to \nu$, respectively. We have made sure that the definitions and the normalizations of these dissipation parameters are the same in the two codes.

Although CLT and M3D-C1 use the same physical model and cylindrical coordinate (R, φ, Z) to solve the toroidal tokamak geometry problems, the code implementations are different. Firstly, the two codes adopt different methods for spatial discretization. The CLT code uses the fourth-order finite difference method in the R, φ, and Z directions, while the M3D-C1 code uses high-order triangular elements with continuous first derivatives (C^1 continuity) in the R and Z directions, and Hermite cubic finite elements in the φ direction [17]. In CLT, the grids are usually not located at the plasma boundary, which is a problem for code development. In the early version of CLT, we applied an interpolation method to solve the boundary problem [29]. However, this method reduces the parallel efficiency of the computation. Therefore, in the new version of the CLT code, we employ the cut-cell method [30] that is more efficient for parallelization. The schematic diagram of the cut-cell method is shown in Fig. 1. Along with the cut-cell method, we have also applied the OpenACC heterogeneous parallel programming model into the code, which typically makes the code 200 times faster [19]. The time advance methods in the two codes are also different. In CLT, the fourth-order accuracy Runge-Kutta explicit scheme is used for time advancing, while the θ-implicit method is used in M3D-C1 [17].

3. Benchmarking results

This subsection describes the linear and nonlinear benchmark between CLT and M3D-C1 for two major tokamak instabilities: the $m/n = 2/1$ tearing mode and the $m/n = 1/1$ resistive-kink mode.
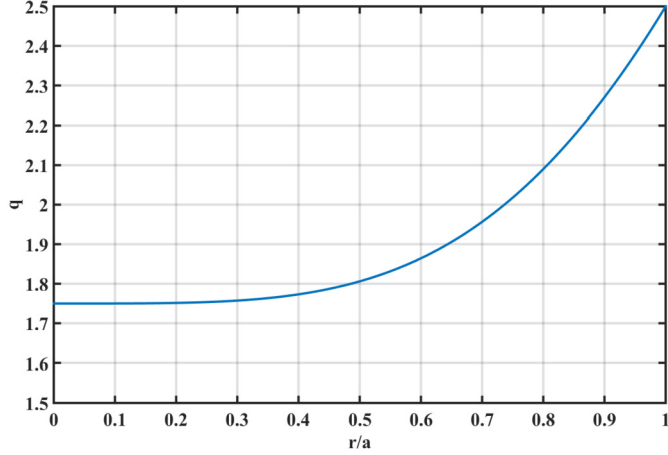
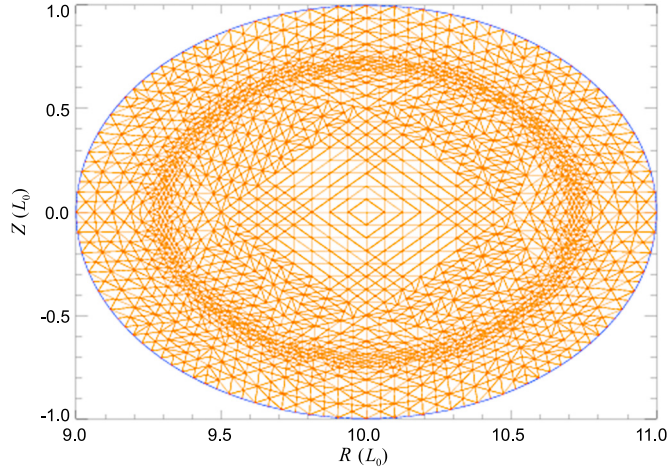**Fig. 2.** The initial safety factor profile used in the $m/n = 2/1$ tearing mode benchmark.

Fig. 3. The non-uniform mesh used in the simulation of M3D-C1. We have packed the mesh around the $q = 2$ resonant surface during the simulation.

3.1. The $m/n = 2/1$ tearing mode

The initial safety factor profile for the $m/n = 2/1$ tearing mode benchmark is shown in Fig. 2. The formula used for the q-profile is given as follows:

$$q = q_0 \times (1 + (\psi_n/q_l)^\alpha)^{1/\alpha}, \tag{1.7}$$

where ψ_n is the normalized poloidal flux, $q_0 = 1.75$, $q_e = 2.5$, $\alpha = 2.0$, $q_l = [(q_e/q_0)^\alpha - 1]^{-1/\alpha}$, and $r = \sqrt{\psi_n}$. For simplification, the plasma beta and the aspect ratio are set to be $\beta \sim 0$ and $R/a = 10/1$ ($a = 1m$). The initial equilibrium is calculated by the QSOLVER code [31]. The dominant MHD instability in the system is the $m/n = 2/1$ tearing mode.

The non-uniform mesh used in M3D-C1 is shown in Fig. 3. During the simulation, we pack the mesh around the $q = 2$ resonant surface to accurately simulate the current sheet of the $m/n = 2/1$ tearing mode. A total of 4800 elements in the poloidal plane and
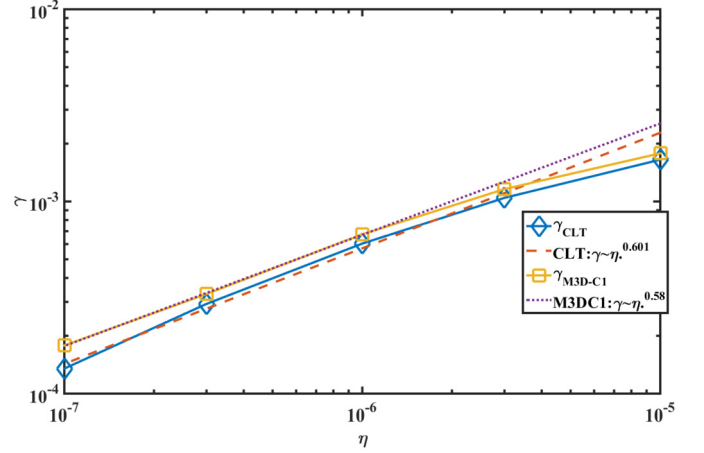

Fig. 4. The scaling laws of the linear growth rates on the resistivity for the tearing mode in CLT and M3D-C1.

16 toroidal planes are used in the nonlinear simulations. The 2D-complex version of M3D-C1 is used for the linear simulation, and the 3D nonlinear version is used for the nonlinear simulation. In CLT, the uniform mesh with $256 \times 16 \times 256$ (R, φ, Z) is used both for the linear and nonlinear simulations.

We start with the linear benchmark of the two codes. Note that the rule for deriving the scaling law for the tearing mode or the resistive-kink mode is that the diffusion parameters are chosen to be much smaller than the resistivity. The diffusion parameters used in the linear benchmark are $D = 1.0 \times 10^{-8}$, $\nu = 1.0 \times 10^{-8}$, $\kappa_\perp = 1.0 \times 10^{-8}$, $\kappa_{||} = 1.0$. For simplification, we choose a constant resistivity and scan from $\eta = 1.0 \times 10^{-5}$ to $\eta = 1.0 \times 10^{-7}$. The linear growth rates of the $m/n = 2/1$ tearing mode with different resistivity are shown in Table 1. The difference between the linear growth rates from the two codes is about 10% for each case.

As shown in Fig. 4, the scaling laws for the linear growth rate with the resistivity are $\gamma \sim \eta^{0.601}$ in CLT and $\gamma \sim \eta^{0.58}$ in M3D-C1, which are both close to the asymptotic theoretical prediction [9,32], i.e., $\gamma \sim \eta^{3/5}$. We use the linear toroidal electric field to represent the mode structure for comparison of the eigenfunctions from the two codes. As shown in Figs. 5a and 5b, the mode structures from the two codes are very similar, and both are the typical mode structures of the $m/n = 2/1$ tearing mode.

The linear benchmark of the $m/n = 2/1$ tearing mode indicates that both codes work well in the linear simulation of the tearing mode. To ease computational requirements, we choose the constant resistivity $\eta = 1.0 \times 10^{-5}$ during the nonlinear simulations.

The nonlinear evolution of the kinetic energy for the $m/n = 2/1$ tearing mode from the two codes is shown in Fig. 6. The dominant mode in the system is the $n = 1$ mode, and its amplitude is much larger than other harmonics. In the nonlinear stage, the tearing mode finally saturates. The saturation level of the $n = 1$ mode for the tearing mode in CLT is about 1.5×10^{-6}, while it is 1.4×10^{-6} in M3D-C1. The saturation levels for other harmonics from the two codes are also very close to each other.

The nonlinear evolutions of the growth rate for the $m/n = 2/1$ tearing mode from the two codes are shown in Fig. 7. The growth

Table 1
The linear growth rates of the $m/n = 2/1$ tearing mode with different resistivity. The time-steps are $dt \sim 8.5 \times 10^{-3} t_A$ in CLT and $dt = 1.0 t_A$ in M3D-C1, respectively. The difference between the linear growth rates from the two codes is about 10% for each case.

	$\eta = 1 \times 10^{-5}$	$\eta = 3 \times 10^{-6}$	$\eta = 1 \times 10^{-6}$	$\eta = 3 \times 10^{-7}$	$\eta = 1 \times 10^{-7}$
M3D-C1	0.00178	0. 00116	0. 000675	0. 000330	0.000178
CLT	0.00165	0. 00104	0. 000604	0. 000293	0.000135
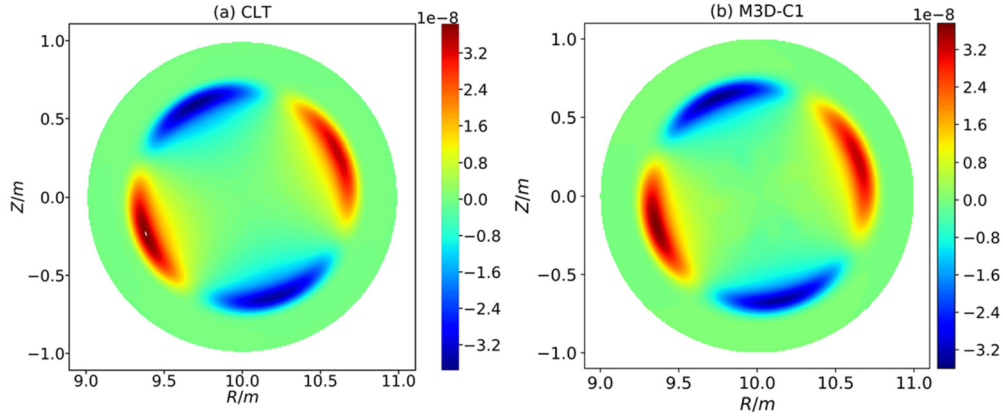
Fig. 5. The toroidal electric field at the linear stage of the simulations (a) CLT and (b) M3D-C1, which represents the mode structure of the $m/n = 2/1$ tearing mode. (For interpretation of the colors in the figure(s), the reader is referred to the web version of this article.)
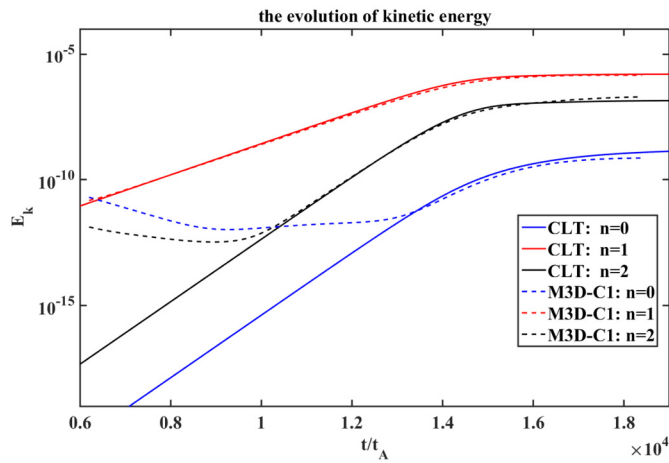

Fig. 6. The nonlinear evolutions of the kinetic energy for the $m/n = 2/1$ tearing mode from the two codes. The results from M3D-C1 are artificially shifted by 4200 t_A for comparison.
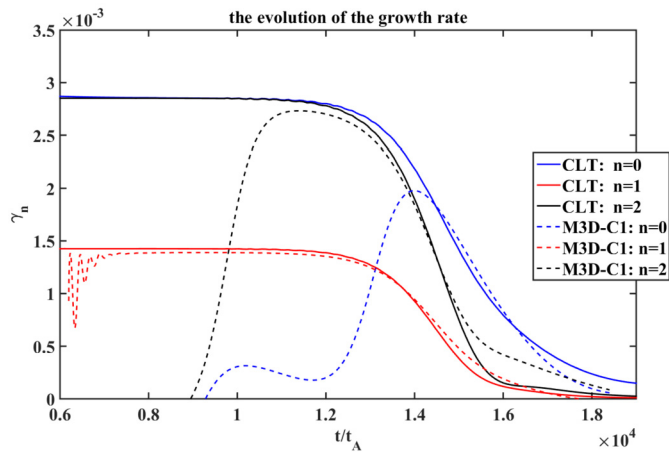
Fig. 7. The nonlinear evolutions of the growth rate for the $m/n = 2/1$ tearing mode from the two codes. The results from M3D-C1 are artificially shifted by 4200 t_A for comparison.

rate of the $n = 1$ mode initially stays almost unchanged during the long linear phase, but slowly reduces in the nonlinear phase, and finally becomes zero when the mode saturates.

In CLT, the initial perturbation only contains the $n = 1$ component, and the $n = 1$ mode is the dominant mode. During the linear stage, the other harmonics are solely driven beat modes of the
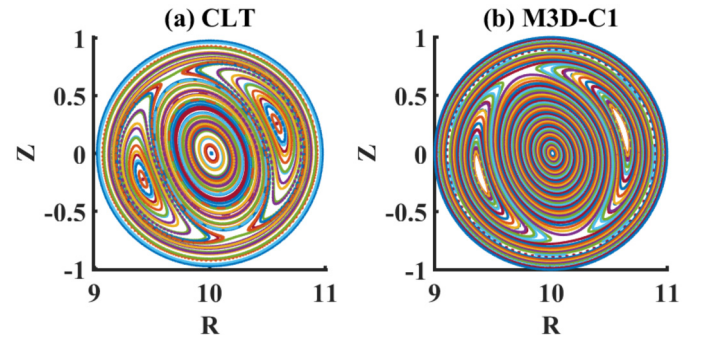
Fig. 8. The Poincare plots of the magnetic field at the saturation stage from the two codes (a) CLT and (b) M3D-C1.

$n = 1$ mode. The growth rates of the $n = 2$ and $n = 0$ modes are twice that of the $n = 1$ mode. In M3D-C1, the initial perturbation is random and contains all components. As a result, modes with different n are present from time zero. They initially decay, but eventually, the harmonic components of the $n = 2$ mode become dominant when the $n = 1$ mode grows to sufficient amplitude. The $n = 0$ mode still independently develops, but its amplitude is much smaller than other modes (Fig. 6) and is not important.

As shown in Fig. 8, the Poincare plots of the magnetic field at the saturation stage from the two codes are almost the same. The mode structures at the saturation stage shown in Fig. 9 (a) CLT and (b) M3D-C1 are very similar.

Although the implementations in CLT and M3D-C1 are different and the tearing mode starts from different initial perturbations, the linear and nonlinear behaviors and the saturation levels of the tearing mode from the two codes agree well with each other. This confirms that CLT and M3D-C1 are both excellent codes for tearing mode studies.

3.2. The $m/n = 1/1$ resistive-kink mode

The initial safety factor profile for the $m/n = 1/1$ resistive-kink mode benchmark is shown in Fig. 10. The formula used in the QSOLVER code is given as follows:

$$q = q_0 + \psi_n[q_e - q_0 + (q'_e - q_e + q_0)(1 - \psi_s)(\psi_n - 1)/(\psi_n - \psi_s)],$$

(1.8)

where $\psi_s = (q'_e - q_e + q_0)/(q'_e + q'_0 - 2q_e + 2q_0)$, $q_0 = 0.7$, $q_e = 3.6$, $q'_0 = 2.0$, and $q'_e = 5.0$. For simplification, the plasma beta and the aspect ratio are set to be $\beta \sim 0$ and $R/a = 10/1$ ($a = 1m$). The initial equilibrium is calculated by the QSOLVER code [31]. The
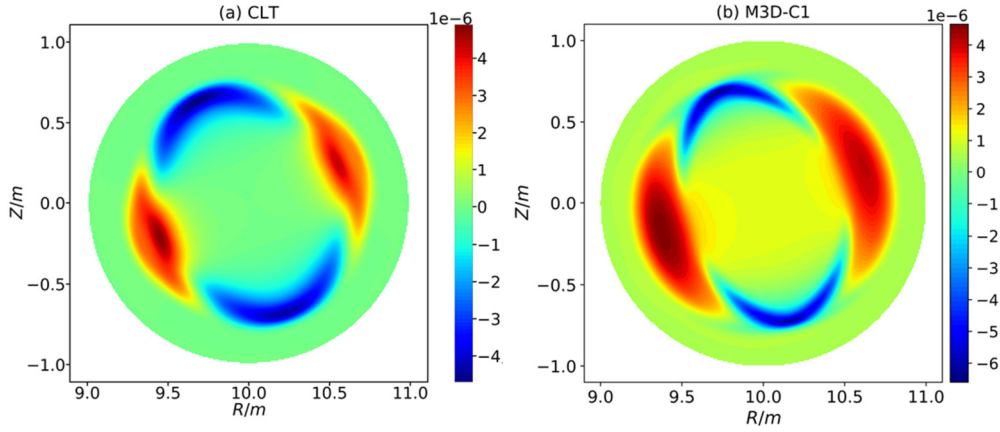
Fig. 9. The mode structures at the saturation stage from the two codes (a) CLT and (b) M3D-C1.
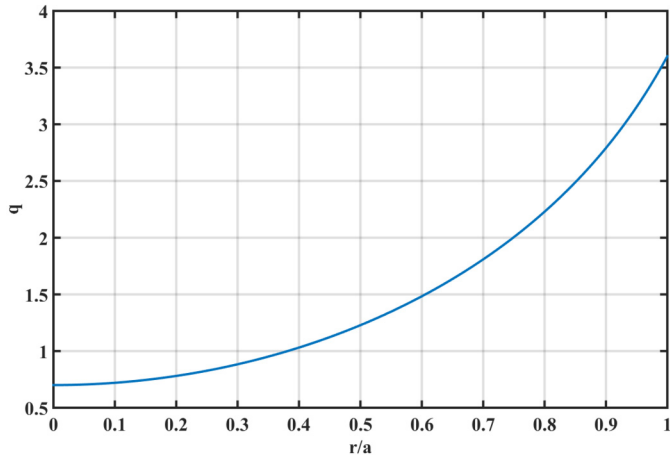

Fig. 10. The initial safety factor profile used in the $m/n = 1/1$ resistive-kink mode benchmark.
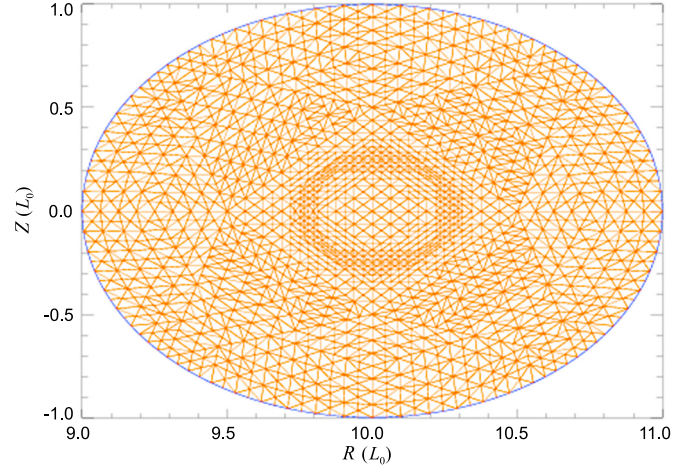

Fig. 11. The non-uniform mesh used in the simulation of M3D-C1. We have dense the mesh around the $q = 1$ resonant surface during the simulation.

$m/n = 1/1$ resistive-kink mode is the dominant mode in the system.

The non-uniform mesh used in M3D-C1 is shown in Fig. 11. We packed the mesh around the $q = 1$ resonant surface to accurately simulate the current sheet of the $m/n = 1/1$ resistive-kink mode. A total of 3816 elements in the poloidal plane and 12 toroidal planes are used in the nonlinear simulations. The 2D-complex version of M3D-C1 is used for the linear simulation, and the 3D nonlinear version is used for the nonlinear simulation. In CLT, the uniform mesh with $256 \times 12 \times 256$ (R, φ, Z) is used both for the linear and nonlinear simulations.

Before the nonlinear benchmark, a systematical linear scan with the two codes is carried out. The diffusion parameters used in the linear simulations are $D = 1.0 \times 10^{-8}$, $\nu = 1.0 \times 10^{-8}$, $\kappa_\perp = 1.0 \times 10^{-8}$, $\kappa_{||} = 1.0$. For simplification, we choose a constant resistivity and scan from $\eta = 1.0 \times 10^{-5}$ to $\eta = 1.0 \times 10^{-7}$. The linear growth rates of the $m/n = 1/1$ resistive-kink mode with different resistivity are shown in Table 2. The difference between the linear growth rates from the two codes is about 5% for each case.

As shown in Fig. 12, the scaling laws for the linear growth rate with the resistivity are $\gamma \sim \eta^{0.31}$ in CLT and $\gamma \sim \eta^{0.30}$ in M3D-C1, respectively, which are both close to the asymptotic theoretical prediction [6], i.e., $\gamma \sim \eta^{1/3}$. A comparison of the linear mode structures is shown in Fig. 13. The mode structures in the two codes are both very similar to the typical mode structure of the $m/n = 1/1$ resistive-kink mode.

To again ease computing requirements, we choose a constant resistivity $\eta = 1.0 \times 10^{-5}$ in the nonlinear simulations. The dominant mode is the $n = 1$ mode, and its amplitude is much larger than other harmonics. As shown in Fig. 14, the nonlinear evolution of the kinetic energy for the $m/n = 1/1$ resistive-kink mode from the two codes is almost the same. During the nonlinear stage, the kinetic energy increases, saturates, and then decreases. The maximum value of the kinetic energy of the $n = 1$ mode for the resistive-kink mode is 4.4×10^{-5} in CLT, while it is 4.2×10^{-5} in M3D-C1. The behavior of the other harmonics in the two codes is also very similar.

Table 2
The linear growth rates of the $m/n = 1/1$ resistive-kink mode with different resistivity. The time-steps are $dt \sim 8.5 \times 10^{-3} t_A$ in CLT and $dt = 1.0 t_A$ in M3D-C1, respectively. The difference between the linear growth rates from the two codes is about 5% for each case.

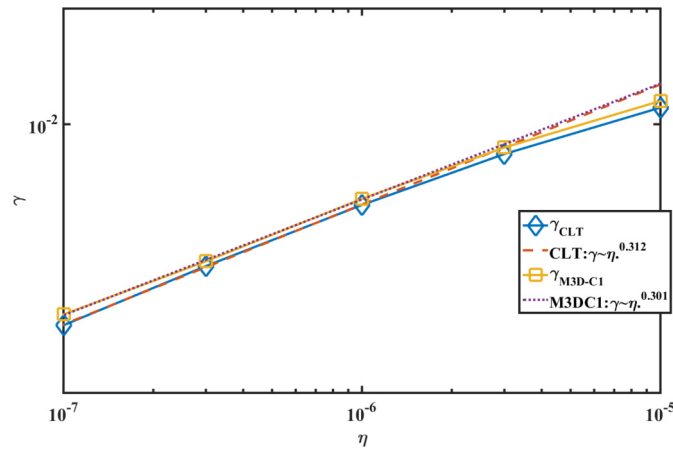|	$\eta = 1 \times 10^{-5}$	$\eta = 3 \times 10^{-6}$	$\eta = 1 \times 10^{-6}$	$\eta = 3 \times 10^{-7}$	$\eta = 1 \times 10^{-7}$
M3D-C1	0. 0115	0. 00870	0. 00640	0. 00440	0.00320
CLT	0. 0111	0. 00837	0. 00617	0. 00428	0.00300

Fig. 12. The scaling laws of the linear growth rates on the resistivity for the resistive-kink mode in CLT and M3D-C1.
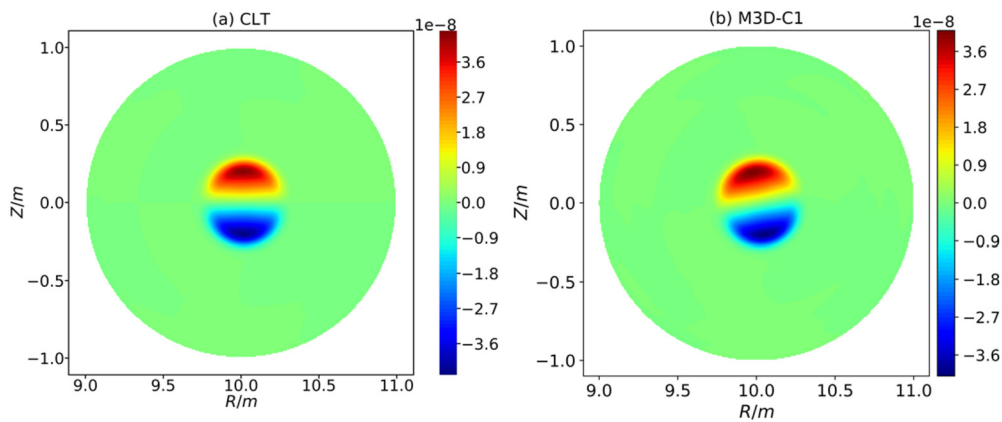

Fig. 13. The toroidal electric field at the linear stage of the simulations (a) CLT and (b) M3D-C1, which represents the mode structure of the $m/n = 1/1$ resistive-kink mode.
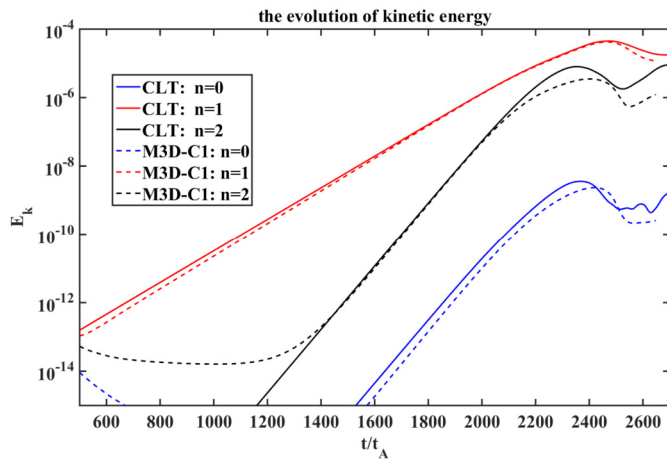

Fig. 14. The nonlinear evolutions of the kinetic energy for the $m/n = 1/1$ resistive-kink mode from the two codes. The results from M3D-C1 are artificially shifted by 270 t_A for comparison.
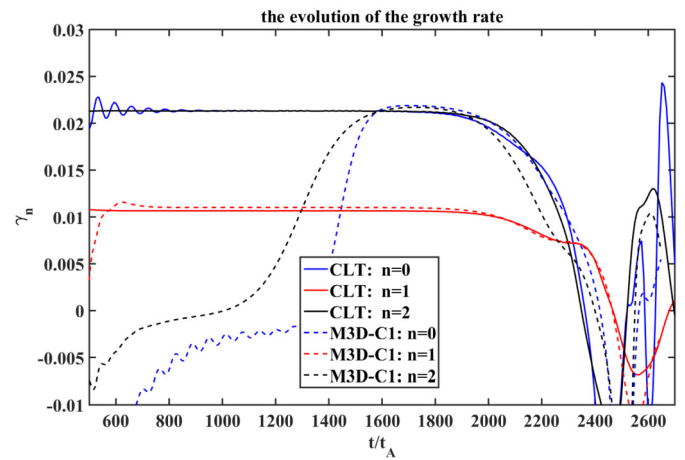

Fig. 15. The nonlinear evolutions of the growth rate for the $m/n = 1/1$ resistive-kink mode from the two codes. The results from M3D-C1 are artificially shifted by 270 t_A for comparison.

As shown in Fig. 15, the growth rates of the $n = 1$ mode initially stay almost unchanged during the long linear phase, then slowly reduces in the early nonlinear phase, and then suddenly reduces to a negative value. It should be pointed out that the evolution of the growth rates is still qualitatively the same even after the crash.

The Poincare plots of the magnetic field during the nonlinear stage from the two codes are shown in Fig. 16 (a) CLT and (b) M3D-C1. They are almost the same. The corresponding mode structures are shown in Fig. 17 (a) CLT and (b) M3D-C1.

Thus, although the CLT code and the M3D-C1 code are very different, the linear and nonlinear behaviors and the maximum kinetic energy of the resistive-kink mode from the two codes are almost the same. This gives confidence in the simulation results of the resistive-kink mode.

4. Summary and discussion

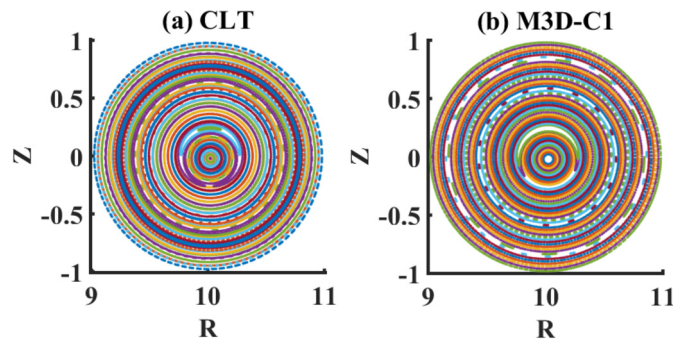In the present paper, we presented a systematic benchmark between the CLT code and the M3D-C1 code for the linear and

Fig. 16. The Poincare plots of the magnetic field at the nonlinear stage from the two codes (a) CLT and (b) M3D-C1.
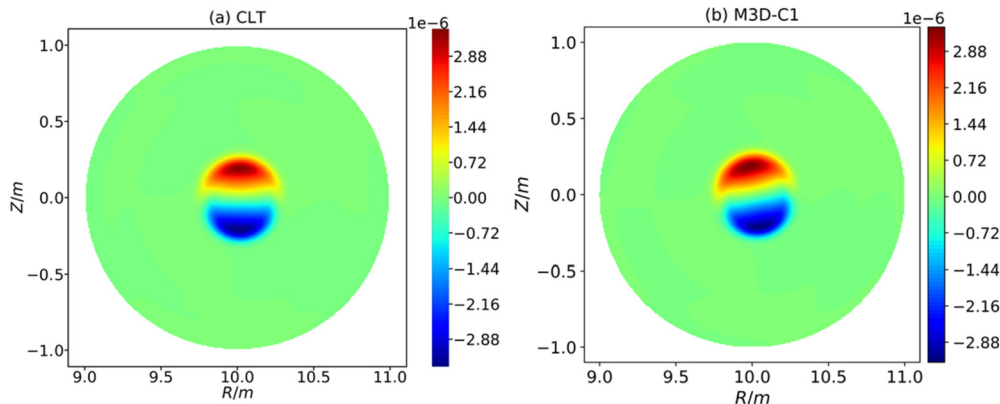

Fig. 17. The toroidal electric field at the nonlinear stage from the two codes (a) CLT and (b) M3D-C1.

nonlinear tearing mode and resistive-kink mode. We find that very similar simulation results for the resistive-kink mode and the $m/n = 2/1$ tearing mode are obtained from the two codes. We compared the linear and nonlinear growth rates, the mode structures, the nonlinear saturation levels, the Poincare plots, and the scaling laws.

CLT is an explicit finite difference code, while M3D-C1 is an implicit finite element code. Although they are both used to investigate MHD instabilities in tokamaks, they are totally different in the code implementations. As presented in the present paper, the simulation results for the $m/n = 2/1$ tearing mode and the resistive-kink mode from the two codes are very close. This gives us confidence in the nonlinear results of the two codes for this class of problems.

It should be noted that the simulation results from the two codes are not exactly the same. There are two possible reasons for the slight difference between the simulation results. The first reason is that the initial perturbations are not the same. In CLT, the initial perturbation only contains the $n = 1$ component, while, in M3D-C1, random perturbations (including all the components) are applied. This is why the development of the harmonics is significantly different at the beginning of the simulations. However, the initial perturbations hardly influence the linear growth rate and the nonlinear evolution of the resistive-kink mode and the $m/n = 2/1$ tearing mode. The second reason is that, due to the different methodologies of the two codes, the initial equilibrium profiles are slightly different. M3D-C1 first reads the initial profiles from the QSOLVER code, solves the Grad-Shafranov equation, and then generates equilibrium consistent with its finite element representation before the simulation. However, the CLT code does not solve the Grad-Shafranov equation. CLT reads the equilibrium data from the QSOLVER code [31] and directly interpolates the data into its mesh. This means that the initial equilibria used in the two

codes are slightly different, which could be why the nonlinear evolution is not exactly the same.

The initial equilibriums used in the simulations are both with the low-beta limit ($\beta \sim 0$) and large aspect ratio ($R/a = 10/1$), while, in typical Tokamaks, the plasma beta is a few percent and the aspect ratio is from $R/a \sim 3/1$ to $R/a \sim 4/1$. With these equilibriums, we can not only benchmark the simulation results with each other, but also benchmark our simulation results with theoretical predictions, i.e. the scaling law of the tearing mode is $\gamma \sim \eta^{3/5}$ [9], and it is $\gamma \sim \eta^{1/3}$ [6] for the resistive-kink mode. As a result, this type of initial equilibriums is often adopted for benchmarking studies between different Tokamak simulation codes, and this is the reason why we choose such equilibriums in our simulations. It should also be aware that with the finite plasma beta, the MHD activities in Tokamaks could be significantly different, and the thermal conductivities $\kappa_\|$ and $\kappa_\perp$ then become crucial. The aspect ratio determines the coupling between the modes with different poloidal modes, and this can also be important for Tokamaks. More complicated benchmarks between the CLT code and the M3D-C1 code with finite plasma beta and aspect ratio are then needed for further validating the two codes in the real Tokamak parameter regime, and will be carried out in the future.

Declaration of competing interest

The authors declare that they have no known competing financial interests or personal relationships that could have appeared to influence the work reported in this paper.

Acknowledgement

References

[1] T.C. Hender, J.C. Wesley, J. Bialek, A. Bondeson, A.H. Boozer, R.J. Buttery, A. Garofalo, T.P. Goodman, R.S. Granetz, Y. Gribov, O. Gruber, M. Gryaznevich, G. Giruzzi, S. Günter, N. Hayashi, P. Helander, C.C. Hegna, D.F. Howell, D.A. Humphreys, G.T.A. Huysmans, A.W. Hyatt, A. Isayama, S.C. Jardin, Y. Kawano, A. Kellman, C. Kessel, H.R. Koslowski, R.J.L. Haye, E. Lazzaro, Y.Q. Liu, V. Lukash, J. Manickam, S. Medvedev, V. Mertens, S.V. Mirnov, Y. Nakamura, G. Navratil, M. Okabayashi, T. Ozeki, R. Paccagnella, G. Pautasso, F. Porcelli, V.D. Pustovitov, V. Riccardo, M. Sato, O. Sauter, M.J. Schaffer, M. Shimada, P. Sonato, E.J. Strait, M. Sugihara, M. Takechi, A.D. Turnbull, E. Westerhof, D.G. Whyte, R. Yoshino, H. Zohm, the Itpa Mhd, Nucl. Fusion 47 (2007) S128.
[2] Z. Chang, J.D. Callen, E.D. Fredrickson, R.V. Budny, C.C. Hegna, K.M. McGuire, M.C. Zarnstorff, T. group, Phys. Rev. Lett. 74 (1995) 4663–4666.
[3] O. Sauter, E. Westerhof, M.L. Mayoral, B. Alper, P.A. Belo, R.J. Buttery, A. Gondhalekar, T. Hellsten, T.C. Hender, D.F. Howell, T. Johnson, P. Lamalle, M.J. Mantsinen, F. Milani, M.F.F. Nave, F. Nguyen, A.L. Pecquet, S.D. Pinches, S. Podda, J. Rapp, Phys. Rev. Lett. 88 (2002) 105001.
[4] R.J. Buttery, T.C. Hender, D.F. Howell, R.J.L. Haye, O. Sauter, D. Testa, Nucl. Fusion 43 (2003) 69.
[5] B. Kadomtsev, Sov. J. Plasma Phys. 1 (1975) 389–391.
[6] B. Coppi, R. Galvao, R. Pellat, M. Rosenbluth, P. Rutherford, Fiz. Plazmy 2 (1976) 961–966.
[7] Y.X. Wan, J.G. Li, Y. Liu, X.L. Wang, C. Vincent, C.G. Chen, X.R. Duan, P. Fu, X. Gao, K.M. Feng, S.l. Liu, Y.T. Song, P.D. Weng, B.N. Wan, F.R. Wan, H.Y. Wang, S.T. Wu, M.Y. Ye, Q.W. Yang, G.Y. Zheng, G. Zhuang, Q. Li, C. team, Nucl. Fusion 57 (2017) 102009.
[8] R. Aymar, P. Barabaschi, Y. Shimomura, Plasma Phys. Control. Fusion 44 (2002) 519.
[9] H.P. Furth, J. Killeen, M.N. Rosenbluth, Phys. Fluids 6 (1963) 459–484.
[10] P.H. Rutherford, Phys. Fluids 16 (1973) 1903–1908.
[11] R.B. White, D.A. Monticello, M.N. Rosenbluth, B.V. Waddell, Phys. Fluids 20 (1977) 800–805.
[12] F. Porcelli, D. Boucher, M.N. Rosenbluth, Plasma Phys. Control. Fusion 38 (1996) 2163.
[13] R.E. Denton, J.F. Drake, R.G. Kleva, D.A. Boyd, Phys. Rev. Lett. 56 (1986) 2477–2480.
[14] A.Y. Aydemir, J.C. Wiley, D.W. Ross, Phys. Fluids, B Plasma Phys. 1 (1989) 774–787.
[15] H. Lütjens, J.-F. Luciani, J. Comput. Phys. 229 (2010) 8130–8143.
[16] C.R. Sovinec, J.R. King, J. Comput. Phys. 229 (2010) 5803–5819.
[17] S.C. Jardin, N. Ferraro, X. Luo, J. Chen, J. Breslau, K.E. Jansen, M.S. Shephard, J. Phys. Conf. Ser. 125 (2008) 012044.
[18] O. Czarny, G. Huysmans, J. Comput. Phys. 227 (2008) 7423–7445.
[19] H.W. Zhang, J. Zhu, Z.W. Ma, G.Y. Kan, X. Wang, W. Zhang, Int. J. Comput. Fluid Dyn. 33 (2019) 393–406.
[20] S. Jardin, N. Ferraro, J. Breslau, S. Hudson, D. Pfefferle, B. Tobias, M. Lanctot, Progress on Nonlinear Resistive MHD Code Verification Problems with M3D-C1, DOI, 2016.
[21] I. Krebs, F.J. Artola, C.R. Sovinec, S.C. Jardin, K.J. Bunkers, M. Hoelzl, N.M. Ferraro, Phys. Plasmas 27 (2020) 022505.
[22] B.C. Lyons, C.C. Kim, Y.Q. Liu, N.M. Ferraro, S.C. Jardin, J. McClenaghan, P.B. Parks, L.L. Lao, Plasma Phys. Control. Fusion 61 (2019) 064001.
[23] N.M. Ferraro, B.C. Lyons, C.C. Kim, Y.Q. Liu, S.C. Jardin, Nucl. Fusion 59 (2018) 016001.
[24] N.M. Ferraro, S.C. Jardin, P.B. Snyder, Phys. Plasmas 17 (2010) 102508.
[25] A.D. Turnbull, N.M. Ferraro, V.A. Izzo, E.A. Lazarus, J.-K. Park, W.A. Cooper, S.P. Hirshman, L.L. Lao, M.J. Lanctot, S. Lazerson, Y.Q. Liu, A. Reiman, F. Turco, Phys. Plasmas 20 (2013) 056114.
[26] Y. Liu, A. Kirk, Y. Gribov, M.P. Gryaznevich, T.C. Hender, E. Nardon, Nucl. Fusion 51 (2011) 083002.
[27] H.W. Zhang, Z.W. Ma, W. Zhang, Y.W. Sun, X. Yang, Phys. Plasmas 26 (2019) 112502.
[28] I. Krebs, S.C. Jardin, S. Günter, K. Lackner, M. Hoelzl, E. Strumberger, N. Ferraro, Phys. Plasmas 24 (2017) 102511.
[29] S. Wang, Z. Ma, Phys. Plasmas 22 (2015) 122504.
[30] L. Duan, X. Wang, X. Zhong, J. Comput. Phys. 229 (2010) 7207–7237.
[31] J. DeLucia, S.C. Jardin, A.M.M. Todd, J. Comput. Phys. 37 (1980) 183–204.
[32] H.P. Furth, P.H. Rutherford, H. Selberg, Phys. Fluids 16 (1973) 1054–1063.